Sigma J Eng Nat Sci, Vol. 44, No. 3, pp. 1888–1902, June, 2026

Sigma Journal of Engineering and Natural Sciences
Web page info: https://sigma.yildiz.edu.tr
DOI: 10.14744/sigma.2026.2070

Research Article

Combined effect of thermo-fluidic and MHD flow of sodium alginate-based tri hybrid Casson nanofluid across a linear stretching sheet with thermal slip influence

N. Ch. RAMGOPAL[1], S. RENUKA[2], Kamatam GOVARDHAN[3], M. KAVITHA[4], A. R. DEEPIKA[4,*]

[1]*Department of Mathematics, Mai Nefhi College of Science, Asmara, 1267, Eritrea*
[2]*Department of Mathematics, Nizam College, Hyderabad, 500001, India*
[3]*Department of Mathematics and Statistics, GITAM Deemed to be University, Hyderabad, 502329, India*
[4]*Department of Mathematics, Global Institute of Engineering and Technology, Moinabad, Hyderabad, 501504, India*

ARTICLE INFO

Article history
Received: 30 September 2025
Revised: 25 November 2025
Accepted: 12 January 2026

Keywords:
Heat Generation; Nusselt Number; Porous Media; Sherwood Number; Sodium Alginate; Thermal Slip, Tri-Hybrid Nanofluid,

ABSTRACT

The usage of Casson tri hybrid nanofluids improves the fuel efficiency and engine operation in automobile engineering, and cooling techniques used for food preservation and processing. This gives an awareness for energy storage systems, heat exchangers and other industrial applications. Current investigation aims to address the consequences of heat generation with thermal slip effects on a steady, incompressible, two-dimensional, laminar flow of tri-hybrid nanofluid over a flat stretching sheet. The resultant nonlinear and highly complicated physical flow is explained by utilizing a Matlab-based robust Runge-Kutta-4 scheme. For higher values of volumetric fraction, the fluid motion decelerated whereas, the concentration diffusion enhanced. By enhancing the volume fraction from 0.01 to 0.03 led to a uniformity in the concentration profile and their interaction within the base fluid has profound effect. Magnifying the porosity number decelerated the tri hybrid Casson nanofluid flow. 20% of aluminium oxide and 40% of Cathode nanotubes in the base fluid enhances the heat transfer rate up to 36.35% which is a good result. Novelty of the existing study is to simplify the former study by considering porosity, heat generation and thermal slip parameters to produce a more refined tri-hybrid Casson nanofluid definition.

Cite this article as: Ramgopal NC, Renuka S, Govardhan K, Kavitha M, Deepika AR. Combined effect of thermo-fluidic and MHD flow of sodium alginate-based tri hybrid Casson nanofluid across a linear stretching sheet with thermal slip influence. Sigma J Eng Nat Sci 2026;44(3):1888–1902.

*Corresponding author.
*E-mail address: deepika.ar2009@gmail.com

This paper was recommended for publication in revised form by Editor-in-Chief Ahmet Selim Dalkilic

Published by Yıldız Technical University Press, İstanbul, Turkey

INTRODUCTION

The research of boundary layer fluid flow across a linear stretching sheet plays a vital part in various applications like instant cooling, aerodynamics, process of condensation metallic plates etc. These kinds of flows have very favorable applications in the polymer sheet extrusion or in the drawing of plastic films. While producing these sheets, melting and stretching issues have been taken into consideration to derive the required thickness. Applications of heat transfer and boundary layer flow have been found in different fields such as cooling of metallic plate, drawing of polymer sheets, extrusion of laments from a die, etc. These fluids are basically used for cooling due to their ample abundance. The theory of boundary layer gives us insight about body shape to avoid the separation of boundary layer.

Nanofluid plays an important role for the development of systems of heat transfer as it demands a solid need for upgrading the simulations of fluid and its alternatives. Nanofluids comprises of solid nanoparticles of Nitrides (AIN), oxides (Al_2O_3, CuO, SiO_2, TiO_2), metals (Al, Cu) or Carbides (SiC) which is suspended in the base fluid like ethylene glycol, water, engine oil, and toluene. Nanofluids possess an exclusive physical and chemical physical feature. These nanoparticles having 5% of the volume fraction are been used in the nanofluids for enrichment of heat transmission. Due to their small size, they flow very effortlessly without clogging. These characteristic features captivated many research scholars to discover the heat transfer effects. Nevertheless, an upsurge in the thermal conductivity can't be wholly credited to thermal conductance of these nanoparticles. Other aspects like nanoparticle size, thermophoresis, shape, temperature, etc. have their impacts. And these features have to be taken into account as industries have to recognize fluids which shall be utilized effectively in the heat transfer also fluids which can be utilized as coolants. Ethylene oil, engine oil, and water have less heat transfer capabilities because of their minor heat transfer features. The researchers have studied the effects of Joule heating and Hall current over a chemically reacting and radiating exponentially stretching sheet along with porous media [1].

Fluids in its pure form, for instance water, oil, ethylene glycol etc have a very little thermal conductance which becomes a drawback in the study of fluid flow. Therefore, to enhance the performance of thermal conductance in pure fluid or base fluid, researchers and scientists have invented various methods and techniques. The researchers have introduced a new technique wherein a small sized particles are been suspended [2]. Such a kind of fluid is said to be a nanofluid which is been used vastly in the industrial applications, for the purpose of cooling of power-plants apparatus and various other electronic devices. During recent times, a lot of research was conducted by the scientists regarding transmission of heat. A numerical review on unsteady finite amplitude with internal heat source and an applied vertical magnetic field [3]. The flow of Cu-water nanofluid in between two squeezing plates was reviewed [4]. And they arrived to a conclusion that the higher volume fraction of nanoparticles and Eckert number could control the thermal conductance. The investigation of the irreversibility generation of the flow system under the impact of thermophoresis, viscosity and magnetic field [5]. A numerical and statistical analysis of MHD flow over a nonlinear curved stretching surface with heat generation [6]. An analysis of titanium alloy and cellulose carboxymethyl hybrid nano liquid over a stretching surface [7]. A full study on Maxwell nanostructure on the flow model with heat source/sink over a stretching sheet was done [8]. The effects of Entropy generation on the Williamson nanofluid flow with porous media was done [9].

The previous studies focussed on the Brownian motion and thermophoretic effects of a Casson based nanofluid. Recently, many scientists have comprehensively analysed the hybrid and trihybrid nanofluid flow in-order to obtain a more refined nanofluid flow with better thermal characteristics. The literature of various researchers portrays that the flow of nanofluid will eventually reduce the heat transfer for varying kind of flow patterns [10-12]. Comprehensive analysis of the higher order chemical reaction on micropolar fluid flow was carried out [13]. Also, comprehensive analysis of the upper convective maxwell hybrid nanofluid flow over a stretching sheet was carried out [14].

Zirconium oxide is a ceramic material with excellent mechanical properties and high resistance to heat. ZrO_2 has multiple applications such as, it can be used as bridges, dental crowns, and implants as it possesses biocompatibility, strength and aesthetic appeal. It can also be utilized as high-performance coatings in engines and turbines. ZrO_2 can be employed in solid oxide fuel cells which converts chemical energy to electrical energy with higher efficiency. Due to its high melting point and resistance to corrosion, ZrO_2 can be used in kilns and furnaces. Aluminium oxide possesses hardness property so it is widely used as abrasive material for cutting, polishing and grinding. Due to its excellent insulating properties, Al_2O_3 is used in electrical components, substrates for semiconductors, and capacitors. Al_2O_3 can be employed in biomedical devices such as in prosthetics and orthopaedic implants. It can also be used in manufacturing industrial ceramics for cutting tools, nozzles and bearings. Carbon Nanotubes(CNT) are cylindrical nanostructures made of carbon atoms. They are used in the development of highly sensitive electronic devices and biosensors as it possesses excellent electrical conductivity. CNTs are incorporated in metals, polymers, ceramics, etc to create nanocomposites with enhanced mechanical, thermal and electrical properties. It can also be used in making high performance batteries, supercapacitors and other energy storage devices due to its large surface area. In the biomedical field, CNT's have potential application in imaging , drug delivery, and scaffolds for tissue engineering. It is used as heat sinks and cooling devices because of its high thermal conductivity. ZrO_2, Al_2O_3 and CNT have unique properties such as thermal resistance, biocompatibility, thermal conductivity and high strength which make them indispensable in advancing technologies in various fields. The analysis of viscous fluid flow using neural networks with homogenous and heterogenous reactions was studied [15-16].

Sodium alginate is a type of natural polymer and is a sodium salt in alginic acid which is removed from the cell walls of brown algae. It has been widely used in the food manufacturing, pharmaceuticals, fabric printing, and greasepaints. The utilities of sodium alginate involve intentional embolization, drug distribution system, encapsulation of cells, and cellular therapeutics Barnett [17-26]. The literature presented by scientists clearly illustrates low oscillating magnetic field for a sodium alginate-based hybrid nanofluid flow in between two spinning disks [27]. The work on entropy generation analysis and optimizing mass transfer by examining the effects of endothermic and exothermic reactions was carried out [28].

Based on the cited literature, originality and novelty of present analysis is to simplify the existing investigations by incorporating the trihybrid-nano particles namely ZrO_2, Al_2O_3 and CNT, porosity number, linear sheet expansions, thermal production or annihilation effects along with thermal slip influence and generating more superior solutions of tri-hybrid nano flow, mass and thermal diffusion characteristics inside the coolant systems. Current work shows, the porosity number plays a significant part in the concentration and thermal transmissions in tri-hybrid nanofluids. And comparative analysis with previous outcomes is also presented to display accuracy of attained similar results and is in good agreement.

The fundamental equations for Casson fluid model are be given by

$$\tau_{ij} = \begin{cases} \left(\mu_c + \frac{P_s}{\sqrt{2\pi}}\right) 2e_{ij}\,, & \pi > \pi_0 \\ \left(\mu_c + \frac{P_s}{\sqrt{2\pi_0}}\right) 2e_{ij}\,, & \pi < \pi_0 \end{cases}$$

where the fluid's yield stress is considered as as $P_s = e_{ij}\, e_{ij}$ and e_{ij} represents the rate of deformation at the (i,j)th component.

π - product of rate of deformation multiplied to itself,

π_0 - product's critical value which is based on non-Newtonian model,

μ_c- the non-Newtonian fluids plastic dynamic viscosity.

For $\pi < \pi_0$

$$\tau_{ij} = \mu_c \left(1 + \frac{1}{\beta}\right) 2e_{ij}$$

and $\beta = \mu_c \sqrt{2\pi_0}/P_s$ is the Casson parameter.

Table 1. Investigational values of Al_2O_3, ZrO_2, CNT and $C_6H_9NaO_7$

	$K(W/m.K)$	$\rho(kg/m^3)$	$C_p(J/Kg.K))$
$C_6H_9NaO_7$	0.613	989	4,175
Al_2O_3	40	3,970	765
ZrO_2	1.7	5,680	502
CNT	3,007.4	2,100	790

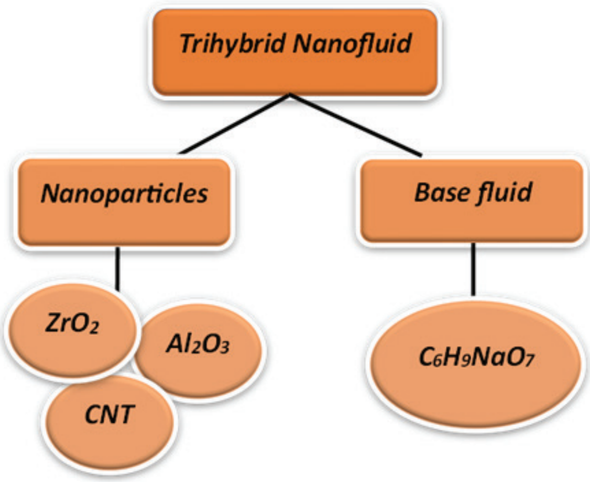

Figure 1. Preparation scheme of tri-hybrid nanoparticles.

Table 2. Thermochemical properties of ternary nanofluids

Viscosity: $$\frac{\mu_{tnf}}{\mu_f} = \frac{1}{(1-\phi_{ZrO_2})^{2.5}(1-\phi_{Al_2O_3})^{2.5}(1-\phi_{CNT})^{2.5}}$$

Density: $$\frac{\rho_{tnf}}{\rho_f} = (1-\phi_{Al_2O_3})\left[(1-\phi_{Al_2O_3})\left\{(1-\phi_{CNT}) + \phi_{CNT}\frac{\rho_{CNT}}{\rho_f}\right\} + \phi_{Al_2O_3}\frac{\rho_{Al_2O_3}}{\rho_f}\right] + \phi_{ZrO_2}\frac{\rho_{ZrO_2}}{\rho_f}$$

Specific Heat: $$\frac{(\rho c_p)_{tnf}}{(\rho c_p)_f} = \phi_{ZrO_2}\frac{(\rho c_p)_{ZrO_2}}{(\rho c_p)_f} + (1-\phi_{ZrO_2})\left[(1-\phi_{Al_2O_3})\left\{(1-\phi_{CNT}) + \phi_{CNT}\frac{(\rho c_p)_{CNT}}{(\rho c_p)_f} + \phi_{Al_2O_3}\frac{(\rho c_p)_{Al_2O_3}}{(\rho c_p)_f}\right\}\right]$$

Thermal Conduction: $$\frac{k_{tnf}}{k_{hnf}} = \left(\frac{k_{CNT} + 2k_{hnf} - 2\phi_{CNT}(k_{hnf} - k_{CNT})}{k_{CNT} + 2k_{hnf} + \phi_{CNT}(k_{hnf} - k_{CNT})}\right), \quad \frac{k_{hnf}}{k_{nf}} = \left(\frac{k_{Al_2O_3} + 2k_{nf} - 2\phi_{Al_2O_3}(k_{nf} - k_{Al_2O_3})}{k_{Al_2O_3} + 2k_{nf} + \phi_{Al_2O_3}(k_{nf} - k_{Al_2O_3})}\right),$$

$$\frac{k_{nf}}{k_f} = \left(\frac{k_{ZrO_2} + 2k_f - 2\phi_{Al_2O_3}(k_f - k_{ZrO_2})}{k_{ZrO_2} + 2k_f + \phi_{Al_2O_3}(k_f - k_{ZrO_2})}\right)$$

Formulation of the Problem

Consider a steady state, incompressible, two-dimensional, linear, laminar, ternary hybrid viscous nanofluid flow across a flat stretching surface. Present mathematical description includes the following assumptions under Prandtl theory predictions:

- Three kinds of nanoparticles namely *CNT*, Al_2O_3, ZrO_2 are been suspended in sodium alginate, which is the base fluid to form a new composition $CNT+Al_2O_3+ZrO_2$ / $C_6H_9NaO_7$ as depicted in Figure 1.
- Rectangular coordinate scheme is preferred. x-axis is along the sheet; y-axis is taken normal to it and the schematic depiction of the physical problem is shown in Figure 2.
- To stabilize the thermal properties and flow of the new composition, the heat generation, thermophoresis, thermal slip and Brownian motion values are been included in flow model.
- Influence of porous media is taken into account in the flow system.
- The flow takes place in a region $y > 0$.
- Flow is created by expanding the sheet along the x-direction with two opposite and equal forces.
- The expansion of the sheet is linear having a velocity as $u_w(x) = ax$ where 'a' is a constant and x represents the obtained coordinate over the linear stretching sheet.
- T_w and C_w temperature and concentration at the stretching surface.
- As $y \to \infty$, the ambient temperature and ambient concentration of the nanoparticles are represented as T_∞ and C_∞ respectively.
- Table 1 presents the investigational values of *CNT*, Al_2O_3, ZrO_2 and $C_6H_9NaO_7$ [29- 31].
- Table 2 presents the thermophysical properties of tri hybrid nanofluids [31-33].

In the light of boundary layer theory assumptions and the foregoing predictions, the present situation yields the following nonlinear partial differential equation [34-35]

$$\frac{\partial u}{\partial x}+\frac{\partial v}{\partial y}=0 \tag{1}$$

$$u\frac{\partial u}{\partial x}+v\frac{\partial u}{\partial y}=\vartheta_{tnf}\left(1+\frac{1}{\beta}\right)\left(\frac{\partial^2 u}{\partial y^2}\right)-\vartheta_{tnf}\left(\frac{u}{k_o}\right) \tag{2}$$

$$u\frac{\partial T}{\partial x}+v\frac{\partial T}{\partial y}=\alpha_{tnf}\frac{\partial^2 T}{\partial y^2}+\tau\left\{D_B\left(\frac{\partial C}{\partial y}\frac{\partial T}{\partial y}\right)+\frac{D_T}{T_\infty}\left[\left(\frac{\partial T}{\partial y}\right)^2\right]\right\}+\frac{Q_o}{(\rho c_p)_{tnf}}(T-T_\infty) \tag{3}$$

$$u\frac{\partial C}{\partial x}+v\frac{\partial C}{\partial y}=D_B\left(\frac{\partial^2 C}{\partial y^2}\right)+\frac{D_T}{T_\infty}\left(\frac{\partial^2 T}{\partial y^2}\right) \tag{4}$$

The imposed boundary conditions for the system of equations are: [37]

$$u=u_w(x), v=-v_w, T=T_w+K_1\frac{\partial T}{\partial y}, \quad C=C_w \text{ at } y=0. \tag{5}$$

$$u=v=0, T=T_\infty, C=C_\infty \text{ as } y\to\infty \tag{6}$$

To complete the mathematical investigation, various quantities are been presented, by using similarity transformations. [37-38].

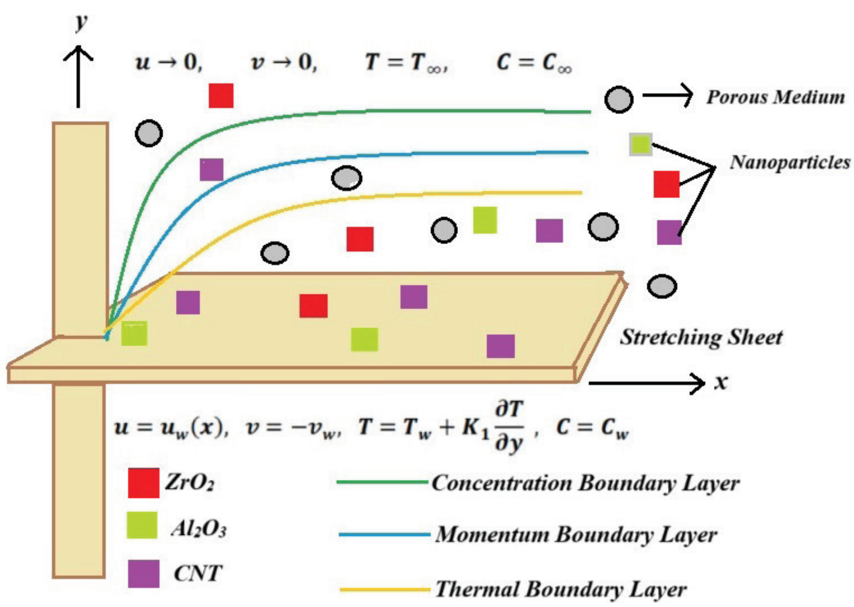

Figure 2. Schematic representation of the physical problem.

$$\left.\begin{aligned} \psi &= \sqrt{a\vartheta}xf(\eta), \\ \eta &= \sqrt{\frac{a}{\vartheta}}y, \\ u &= axf'(\eta), \\ v &= -\sqrt{a\vartheta}f(\eta), \\ \theta(\eta) &= \frac{T-T_\infty}{T_w-T_\infty}, \\ \phi(\eta) &= \frac{C-C_\infty}{C_w-C_\infty} \end{aligned}\right\} \quad (7)$$

Using these transformations, the equations numbered (2) – (4) are Non-linear ODE's.

$$\frac{1}{A_1A_2}\left(1+\frac{1}{\beta}\right)f''' - \frac{1}{A_1A_2}Kf' - ff'' + (f')^2 = 0 \quad (8)$$

$$\frac{A_4}{A_3}\theta'' + Prf' + PrNb\theta'\phi' + PrNt\theta'^2 + Pr\lambda\frac{\theta'}{A_3} = 0 \quad (9)$$

$$\phi'' + Lef\phi' + \left(\frac{Nt}{Nb}\right)\theta' = 0 \quad (10)$$

Here, $A_1 = \frac{\mu_f}{\mu_{tnf}}, A_2 = \frac{\rho_{tnf}}{\rho_f}, A_3 = \frac{(\rho C_p)_{tnf}}{(\rho C_p)_f}, A_4 = \frac{k_{tnf}}{k_f}$ (11)

The related conditions near the boundary are transformed as:

$$\left.\begin{aligned} &f(0) = f_w; f'(0) = 1; \theta(0) = 1 + L\theta'(0); \phi(0) = 1 \text{ at } \eta = 0 \\ &f'(\infty) = 0;\ \theta(\infty) = 0;\ \phi(\infty) = 0 \quad as \quad \eta \to \infty \end{aligned}\right\} \quad (12)$$

f_w represents the value of the function f at the starting point and $f'(0)$ signifies the rate at which the velocity changes at the surface, potentially indicating the behaviour of the fluid moving over the surface. $\theta(0)$ and $\theta'(0)$ has a linear relationship between them and the value of $\phi(0)$ indicates a fixed concentration. $f'(\infty)$ indicates that the gradient or the rate of change of velocity at infinity becomes zero indicating that the flow becomes uniform in that region. $\theta(\infty)$ indicates that the temperature that is far from the boundary approaches the ambient temperature which is assumed to be zero. The value of $\phi(\infty)$ indicates that the concentration vanishes at the boundary. The above-mentioned boundary conditions represent heat transfer problems where the heat is applied at the surface and dissipates as you move far away from the surface.

$$\left.\begin{aligned} &K = \frac{\vartheta}{k_{0a}}, Pr = \frac{\vartheta}{\alpha}, Le = \frac{\vartheta}{D_B}, \lambda = \frac{Q_0}{(\rho c_p)_f a}, L = K_1\sqrt{\frac{a}{\vartheta}}, f_w = -\frac{v_w}{\sqrt{a\vartheta}} \\ &Nb = \frac{(\rho c)_p D_B(\phi_w-\phi_\infty)}{(\rho c)_f\vartheta}, Nt = \frac{(\rho c)_p D_T(T_w-T_\infty)}{(\rho c)_f\vartheta T_\infty} \end{aligned}\right\} \quad (13)$$

Incorporating Eq. (7) in the characterizations of skin friction, rates of thermal and concentration has resulted in the below presented expressions:

$$C_f = \frac{T_w}{\rho u_w^2}, Nu_x = \frac{xq_w}{k(T_w-T_\infty)} \text{ and } Sh_x = \frac{xh_m}{D_B(\phi_w-\phi_\infty)}, \quad (14)$$

$$q_w = -k\left(\frac{\partial T}{\partial y}\right)_{y=0} \text{ and } h_m = -D_B\left(\frac{\partial C}{\partial y}\right)_{y=0} \quad (15)$$

Deployment of Eq. (7) into Eq. (14) and using Eq. (15) gives:

$$C_f\sqrt{Re_x} = -f''(0), \frac{Nu_x}{\sqrt{Re_x}} = -\theta'(0) \text{ and } \frac{Sh_x}{\sqrt{Re_x}} = -h'(0)s. \quad (16)$$

Numericlal Solution

The computational results of the nonlinear ODE's (8) to (10) with its associated boundary conditions in Eq. (12) are numerically solved with shooting approach and integrated Bvp4c solved in MATLAB. For this calculation, the choice of a suitable initial guess value is very crucial as it effects the overall quality. Boundary layer width has an influence on how well the numerical solution performs; thus, it is desired to be chosen wisely into explanation with regard to the problem. To achieve better degree of accuracy, convergence criterion of 10^{-5} is been set. The working mechanism and flow chart of Bvp4c scheme is depicted in Figure 3 [39].

The following predictions on the governing equations:

$$f = y_1,\ f' = y_2,\ f'' = y_3, \theta = y_4,\ \theta' = y_5, \\ \phi = y_6,\ \phi' = y_7. \quad (17)$$

The modified equations are:

$$y_3' = \left(1+\frac{1}{\beta}\right)^{-1}\left[A_1A_2\left(y_1y_3 - f'^2\right) + Ky_2\right] \quad (18)$$

$$y_5' = -Pr\left[\frac{A_3}{A_4}\left(y_2 + Nby_5y_7 + Nty_5{}^2\right) + \frac{\lambda y_4}{A_4}\right] \quad (19)$$

$$y_7' = -\left(Ley_1y_7 + \frac{Nt}{Nb}y_5\right) \quad (20)$$

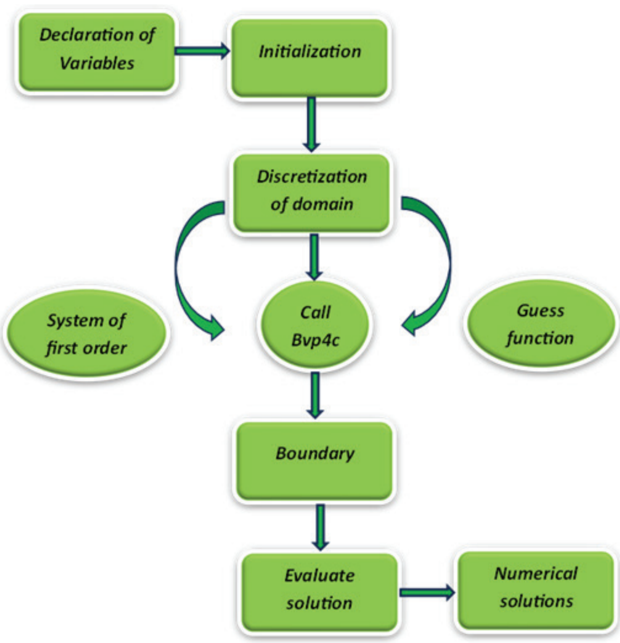

Figure 3. Flow configuration and coordinate system.

Similarly, following boundary conditions are obtained:

$$\left.\begin{array}{c} y_1(0)=f_w, y_2(0)=1, y_4(0)=1+Ly_5(0), y_6(0)=1 \\ y_2(\infty)=0, y_4(\infty)=0, y_6(\infty)=0 \end{array}\right\} \quad (21)$$

The produced results have been depicted through graphs and tables.

RESULTS AND DISCUSSION

The visual representation of Casson Tri-Hybrid nanofluid motion, thermal and mass diffusion for various parametric values is portrayed in the Figs. 4-19, respectively.

CNT + Al_2O_3 + ZrO_2/ $C_6H_9NaO_7$ Tri Hybrid Nanofluid
Al_2O_3 + ZrO_2/ $C_6H_9NaO_7$ Hybrid Nanofluid
ZrO_2/ $C_6H_9NaO_7$ Nanofluid

Velocity Characteristics

Figures 4-6 depicts the velocity $f'(\eta)$ versus Casson fluid parameter (β), porous media (K) and volume fraction (ϕ).

Figure 4 shows a growth in Casson parameter led to a decline in the motion of the fluid. Inclusion of ZrO_2, Al_2O_3 and CNT in the base fluid led to a change in the fluid's viscosity. Due to the hardness and strong bonding of these nanoparticles, the flow resistance increases and thus leading

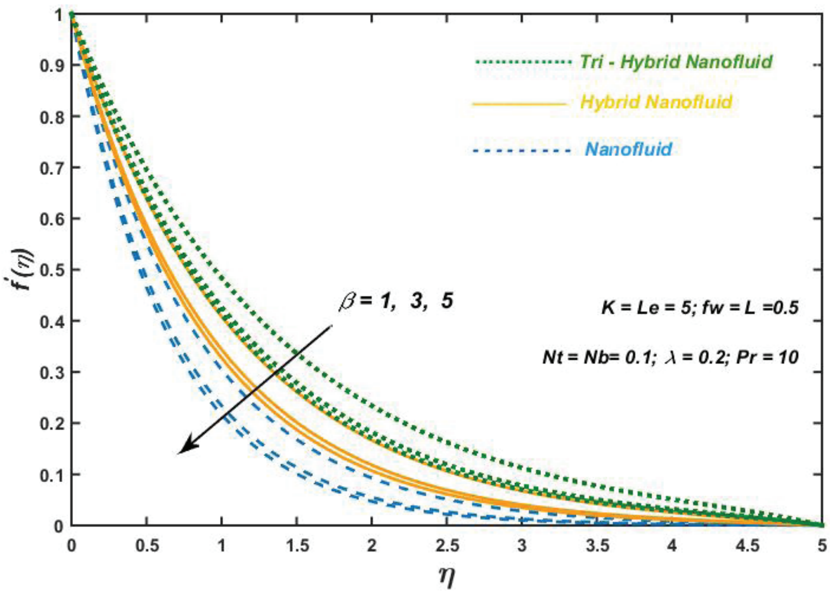

Figure 4. Velocity variations with Casson fluid parameter (β).

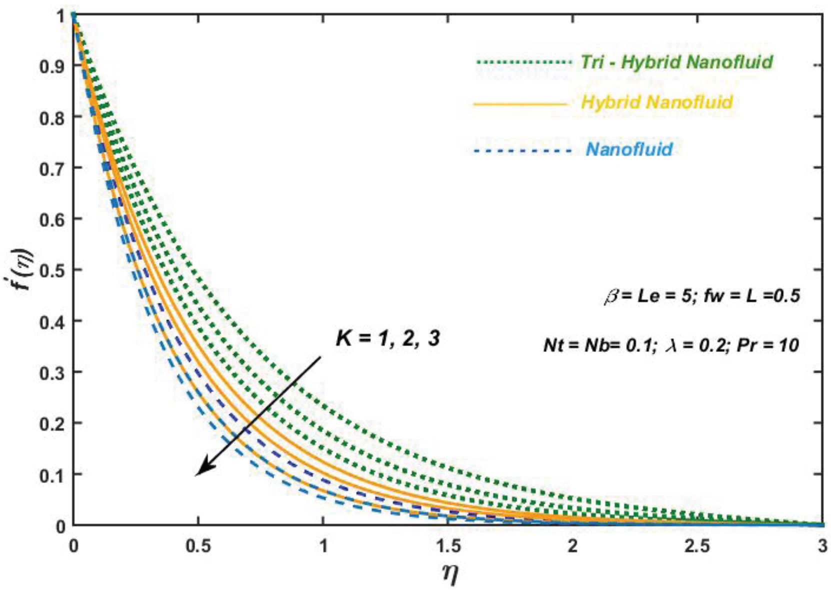

Figure 5. Velocity variations with respect to porous media (K).

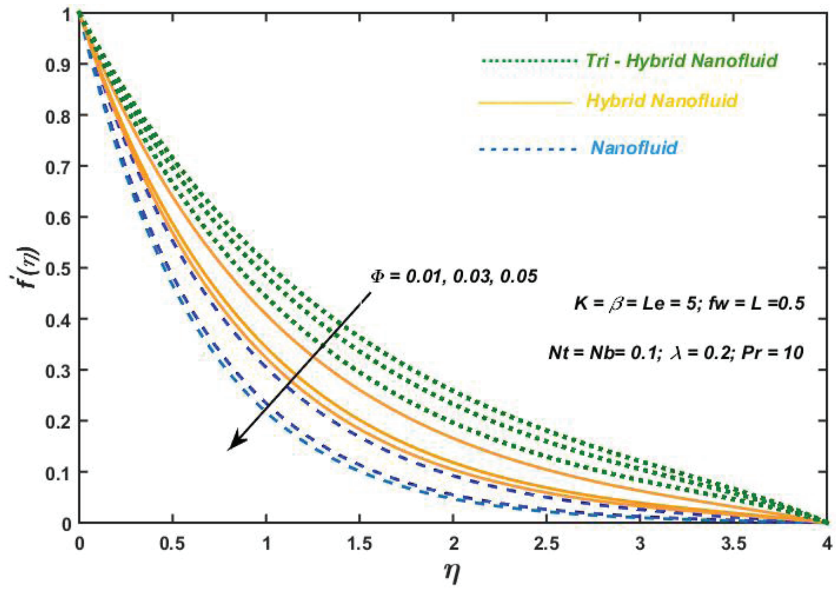

Figure 6. Variation of velocity with respect to volume fraction (ϕ).

to the reduction in velocity. Variation of velocity profiles with porous effects have been depicted in Figure 5 and it displays a falling velocity profile. These nanoparticles cause the viscosity to raise in the base fluid and this phenomenon affects the pressure drop and flow resistance within porous structures. Higher porosity parameter shows the fluid flow via a bigger number of arbitrarily oriented pores, thus dipping its velocity. From Figure 6, velocity declines with the nanoparticle's volume fraction. The trihybrid nature of ZrO_2, Al_2O_3 and CNT can offer synergetic effects in terms of flow resistance resulting in altered velocity profiles. The velocity profile becomes very uneven near the boundary and similar outcomes were seen in the literature [40]. The applications of these trihybrid nanofluid are of prime importance as they exhibit a non-Newtonian behaviour leading to shear thinning and thickening effects. They can be widely used in lubrication systems, heat exchangers, and nanotechnology.

Thermal Characteristics

Figures 7-9 depicts the temperature $\theta(\eta)$ versus heat generation (λ), thermal slip (L), and volume fraction parameters.

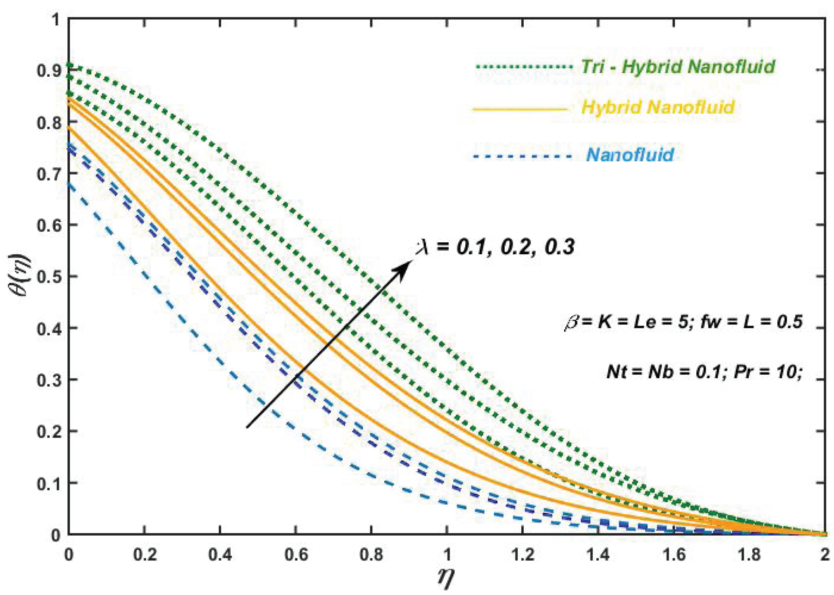

Figure 7. Variation of temperature with respect to heat generation (λ).

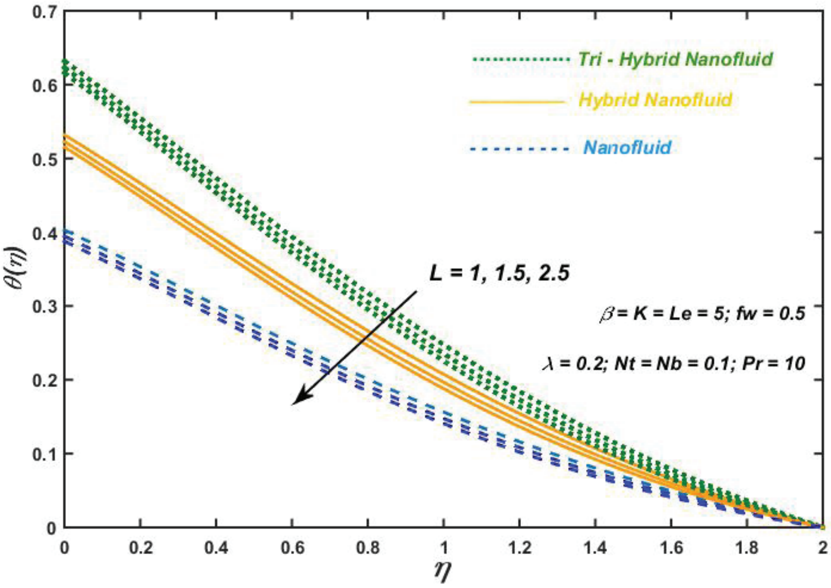

Figure 8. Temperature variations with respect to thermal slip (L).

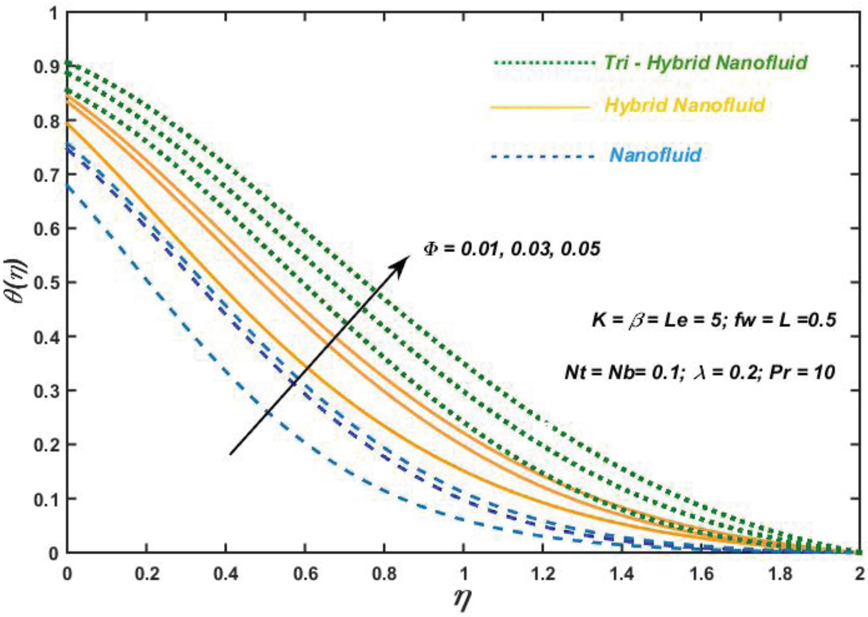

Figure 9. Variation of temperature with respect to volume fraction (ϕ).

Figure 7 shows the significant temperature variations when heat source parameter is increased. Mixture of ZrO_2, Al_2O_3 and CNT nanoparticles allows more uniform temperature distribution across the fluid due to its better thermal conductivity and causing the thermal resistance to reduce. Similar outcomes were observed [40]. In Figure 8, displays the effects of slip parameter on thermal field. Thermal slip refers to the difference in temperature in between surface of the solid nanoparticle and the bulk fluid, caused by reduced thermal resistance near the interface. By introducing the thermal slip boundary condition can significantly affect the temperature distribution within the fluid. It conveys that, an increase in the slip parameter improves the thermal transmission with reduced temperature distribution. Similar results were seen [41]. Figure 9 depicts the effects that the volume fraction has on the temperature. ZrO_2, Al_2O_3 and CNT has high thermal conductivity in comparison with conventional base fluids. When they are combined into a trihybrid nanofluid, their individual the overall heat transfer properties improve. The volume fraction significantly influences the overall thermal conductivity of the nanofluid. An increase in the volume fraction leads to higher thermal profile for the fluid.

Concentration Characteristics

Figures 10-12 depicts the concentration $\emptyset(\eta)$ versus volume fraction ($\emptyset$), Thermophoresis (Nt) and Lewis number (Le).

Figure 10 represents the influence of volume fraction on the concentration profile. By enhancing the volume fraction from 0.01 to 0.03, there is an addition of ternary nanoparticles which causes the concentration profile to become more uniform, and their interaction within the base fluid has profound effect. It is evident that thermophoresis force which is formed due to the gradient in temperature to its free stream value. So, higher values of Nt shows that a greater number of fluid particles would move from the warmer zone to the cooler zone and toughen the species layer thickness as depicted in Figure 11. The effects of

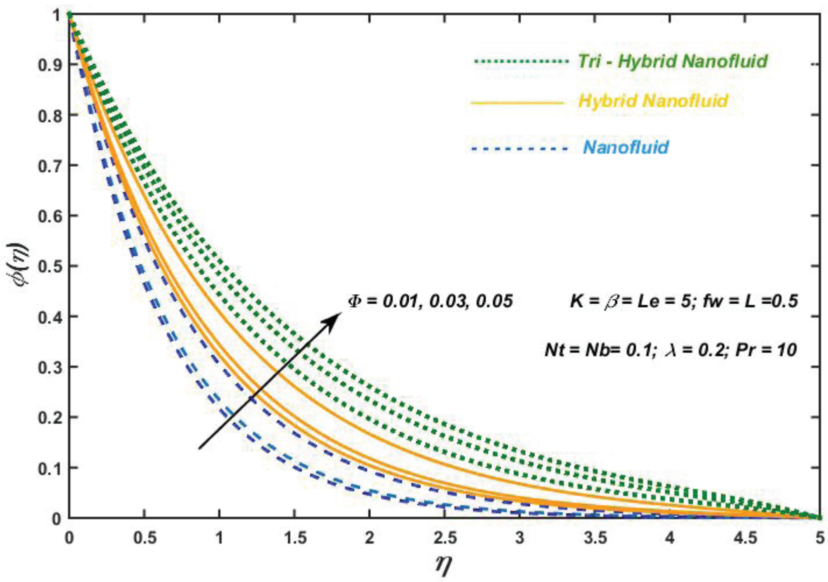

Figure 10. Concentration variations with respect to volume fraction (ϕ).

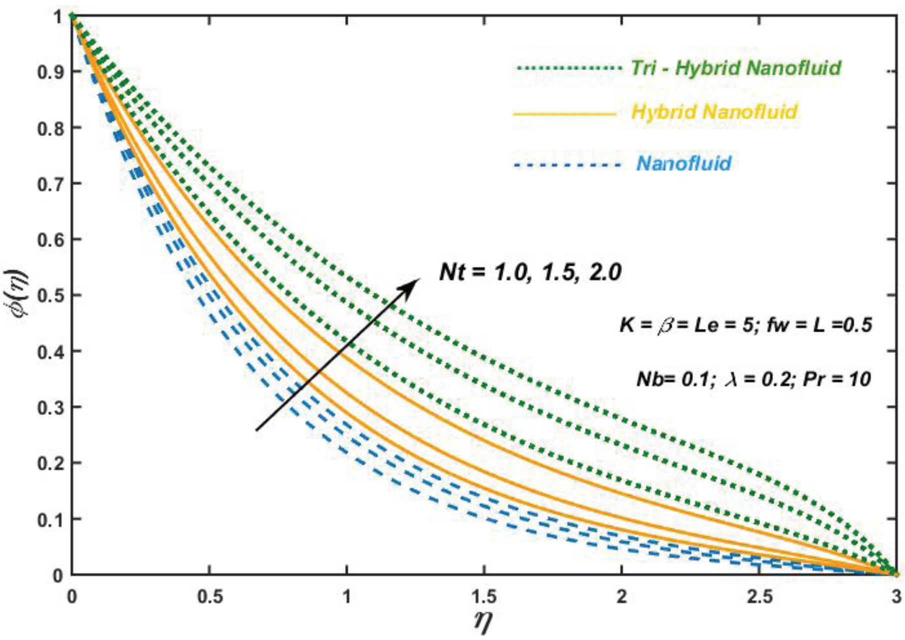

Figure 11. Concentration variations with thermophoresis (Nt).

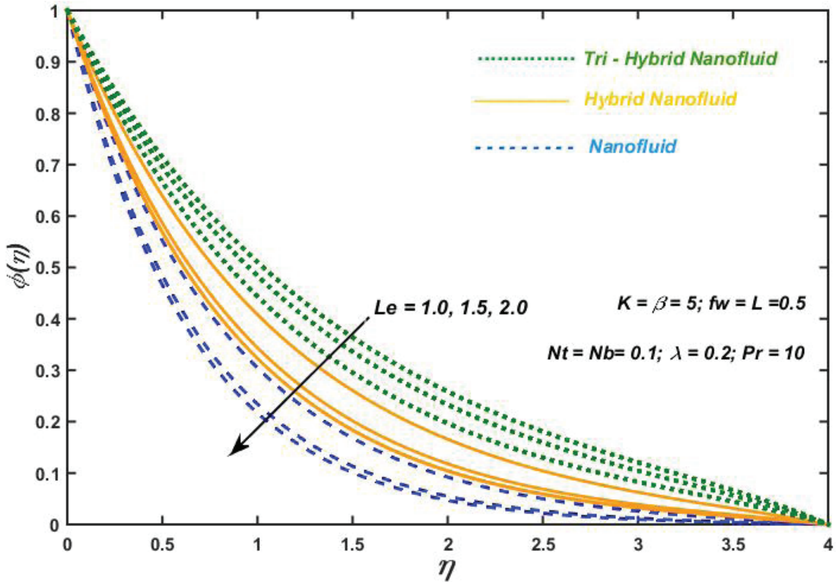

Figure 12. Variation of concentration with respect to Lewis number (*Le*).

higher Lewis number upon $\phi(\eta)$ is depicted in Figure 12. Lewis number is the ratio of thermal diffusivity to mass diffusivity. By enhancing the values of *Le* heat diffusion takes place more rapidly than mass and hence causing the concentration to decay. The volume fraction and Lewis number effects of the trihybrid nanofluid has a significant role on the concentration profile. These can be used in thermal management, Lubrication, and energy storage.

Percentage Variations In Skin Friction

Figures 13-18 depicts the bar graph for skin friction, Nusselt and Sherwood number with several governing parameters.

From Figure. 13, it has been noticed that the porous parameter reduces velocity due drag effects, increasing skin friction. Addition of nanoparticles ZrO_2, Al_2O_3 and CNT increases viscosity which then leads to the enhanced resistance at the surface. From Figure 14, as the volume fraction of the nanoparticles increase, nanofluid viscosity also rises, this leads to momentum diffusion at the surface, enhancing the skin friction. CNT's have high aspect ratios and excellent thermal conductivity and hence contributes to the rise in viscosity compared to ZrO_2 and Al_2O_3 particles. Given the significant impact on skin friction, this nanofluid can be used in Energy systems, biomedical applications, etc.

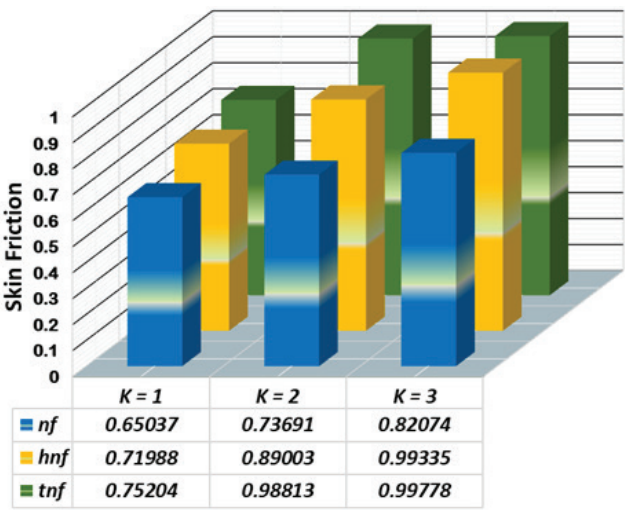

Figure 13. Skin-friction variation with porous parameter.

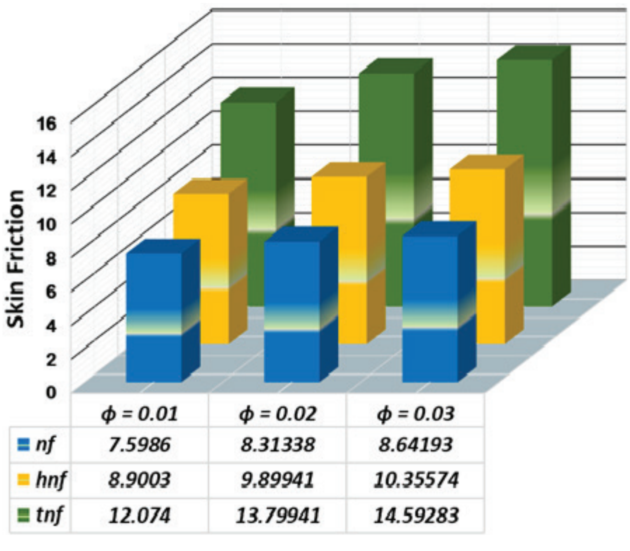

Figure 14. Skin-friction variation with volume fraction ϕ.

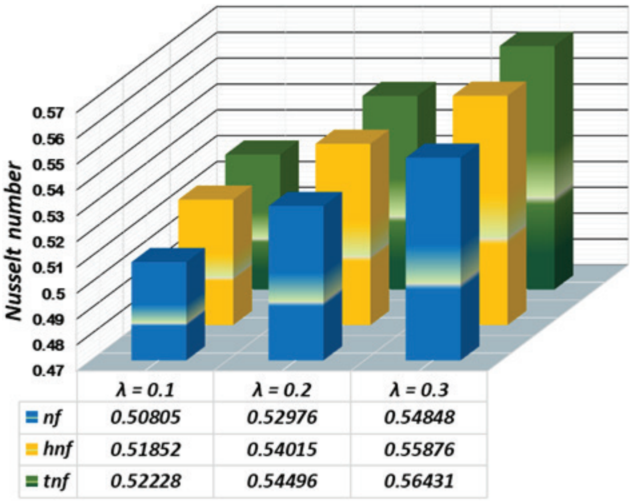

Figure 15. Nusselt number variation with heat source parameter.

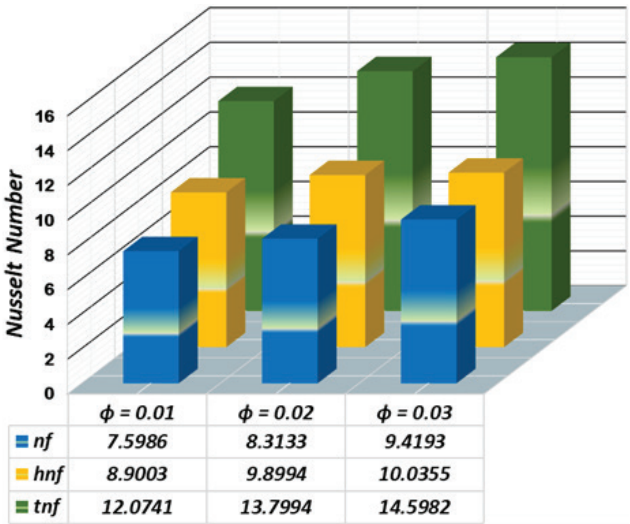

Figure 16. Nusselt number variation with volume fraction ϕ.

Percentage Variations in Nusselt Number

Figure 15 portrays the Nusselt number variations for increasing values of Heat generation (λ). When an internal heat generation parameter is introduced, the temperature gradient increases, impacting the boundary layer thickness. For higher heat generation, the thermal boundary layer expands. CNT's have higher thermal conductivity in comparison with ZrO_2 and Al_2O_3. From Figure 16, the addition of nanoparticles improves the effective thermal conductivity of the base fluid due to their higher intrinsic conductivity. CNTs in particular possess exceptional thermal conductivity (~3000 W/mK) boosting heat transfer efficiency. As the volume fraction upsurges, Nusselt number generally increase due to better thermal diffusion and Brownian motion effects. And similar recordings were found. [42].

Percentage Variations in Sherwood Number

With the raise in heat generation from 0.1 to 0.3, the Sherwood number had enhanced in all the three cases as depicted in Figure. 17. Increasing heat generation, leads to rise in temperature within the field. This reduces fluid viscosity, thereby enhancing convective effect. Enhanced convection results in an increase in Sherwood number. Figure 18 depicts Sherwood number variations with volume fraction. ZrO_2 improves thermal and mechanical

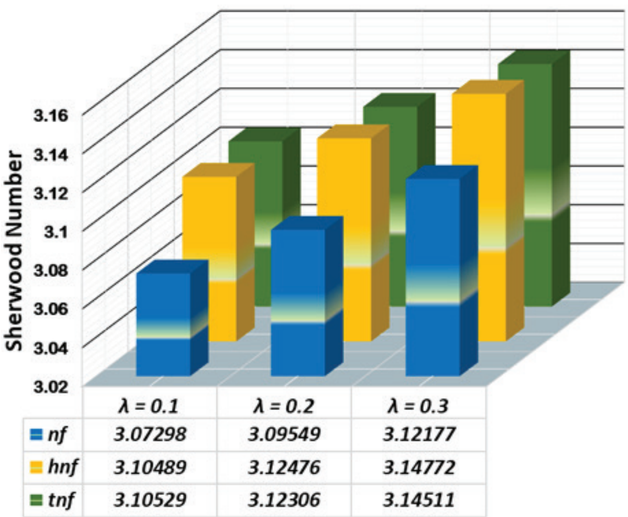

Figure 17. Sherwood number variation with heat source parameter λ.

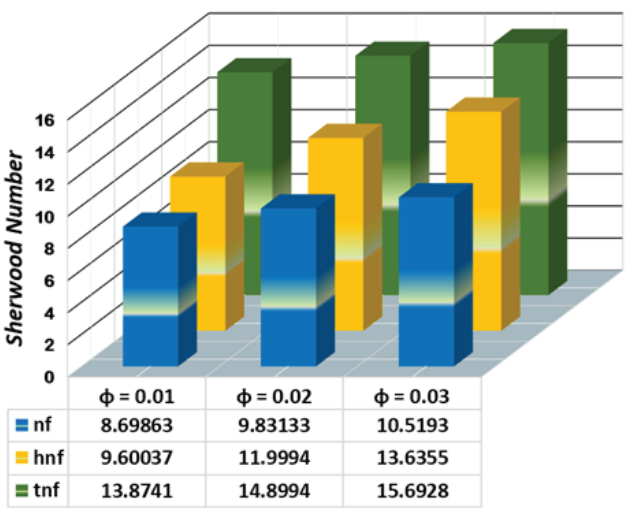

Figure 18. Sherwood number variation with volume fraction ϕ.

Table 3. Simulated Skin-friction values for varying β, K and fw

β	K	fw	$-f''(0)$
1	1	0.5	0.759886
3			0.864193
5			0.895258
	1		0.094355
	2		0.481303
	3		0.759886
		0.5	0.759886
		1.0	0.626806
		1.5	0.521262

stability, enhancing the diffusion process. Al_2O_3 increases heat transfer efficiency and mass diffusion properties. CNTs provide exceptionally high thermal conductivity and contribute to turbulence, enhancing mass transport.

Table 3 shows Skin-friction values by changing β, K and fw. Skin friction was seen to increase for larger values of Casson fluid and porous media parameters while an opposite trend was found in case of suction parameter fw. Table 4 shows the computed Nusselt $-\theta'(0)$ for changing values of Pr, λ and L. As the value of Prandtl number increased, a rise in Nusselt number was seen whereas an opposite trend was found with regard to heat generation and thermal slip parameters. Similar recordings were found in the literature [29]. Table 5 depicts the calculated Sherwood values $-\emptyset'(0)$ by changing values of Le, Nt and Nb. There was a raise in the local Sherwood number for higher values of Lewis number, Thermophoresis and Brownian motion parameters.

Table 6 shows the percentage improvement of Nusselt number with varying values of volume fraction and was found to be in good agreement with the previously published results [31]. Validation of the present work was done when $K=Le=5; fw=L=0.5; Nt=Nb=0.1; \beta \rightarrow \infty$;

Table 4. Computed Nusselt $-\theta'(0)$ for varying values of Pr, λ and L

Pr	λ	L	$-\theta'(0)$
0.7	0.1	1.0	0.478562
1.0			0.509824
3.0			0.707581
	0.1		0.548482
	0.3		0.508051
	0.5		0.451454
		1.0	0.508051
		1.5	0.408471
		2.5	0.291870

Table 5. Computed Sherwood $-\emptyset'(0)$ for varying values of Le, Nt and Nb

Le	Nt	Nb	$-\emptyset'(0)$
1	0.1	0.1	0.388270
1.5			0.731822
2.0			1.079921
	0.5		2.562286
	1.0		2.715077
	2.0		4.223342
		0.5	0.907794
		1.0	1.076257
		2.0	1.125274

Table 6. Comparison of percentage enhancements of Nusselt number

Al_2O_3	*CNT*	*Nusselt Number*	*% Enhancement (Previous Outcome)* [31]	*% Enhancement (Present Outcome)*
0%	0%	0.487	-	-
20%	40%	0.664	36.35%	36.37%
40%	40%	0.647	32.85%	32.85%
40%	20%	0.642	31.83%	31.80%
40%	30%	0.645	32.44%	32.39%
30%	30%	0.653	34.09%	34.10%
30%	40%	0.656	34.70%	34.89%
0%	50%	0.682	40.04%	40.04%
50%	50%	0.642	31.83%	31.99%
50%	0%	0.629	29.16%	29.12%

CONCLUSION

The current study investigates the two-dimensional convective, viscous, steady state Tri-hybrid nanofluid across a flat linear stretching sheet. Nanoparticles namely Zirconium oxide, Aluminium oxide and cathode nanotubes are been suspended in sodium alginate which is the base fluid forms a tri-hybrid nanofluid. The real time applications of this composition is that they are used in Biomedical, Pharmaceutical applications, drug delivery and control release systems. In order to stabilize the thermal and flow features of the newly obtained structure, Brownian and thermophoresis features are combined in the energy and concentration Navier Stokes equations. Porous media and heat generation effects are been incorporated in the momentum and energy equations respectively. All these physical diagrams have various uses in the field of engineering. In the study, a numerical investigation is been done to present the pattern of transmission of velocity, thermal and concentration in tri-hybrid nanofluids upon a flat linear stretching sheet. The significant outcomes of the present study include:

- ❖ With greater values of volume fraction of the nanoparticles, the density of the fluid upsurges which causes more resistance in the fluid motion. Therefore, the fluid motion declines.
- ❖ Flow characteristics have decayed for higher values of porosity and Casson fluid parameter.
- ❖ Thermal characteristics were noted to be amplified with the rise in thermophoresis, heat generation and Brownian motion parameters. The effects were more prominent in the tri-hybrid nanoparticles.
- ❖ Thermal boundary layer was lessened for greater values of Prandtl number and thermal slip parameters.
- ❖ Enhancing the volume fraction and thermophoresis values upsurges the concentration and species boundary layer thickness. Whereas an opposite trend was reported for higher values Lewis number.

NOMENCLATURE

C	Concentration of nano particle
C_w	Concentration at the surface
C_∞	Concentration at infinity
D_B	Coefficient of Brownian flow
D_T	Coefficient of Thermophoresis
fw	Suction
h_f	Heat transfer coefficient
K	Porous media parameter
K_1	Coefficient of Thermal slip
L	Thermal Slip
Nb	Brownian motion parameter
Nt	Thermophoresis parameter
N_∞	Ambient microorganism concentration
Pr	Prandtl number
T_∞	Ambient temperature
T_w	Temperature at the surface

Greek Symbols

η	Dimensionless Similarity variable
β	Casson fluid parameter
λ	Heat source
ρ	Fluid density
π	Deformation rate
σ	Electric conductivity
θ	Dimensionless temperature

Subscripts

f	Nanofluid
tnf	Tri-Hybrid Nanofluid
w	Condition at the wall
∞	Condition at the free stream

AUTHORSHIP CONTRIBUTIONS

N. Ch. Ramgopal: Conceptualization, Data Curation.
S. Renuka: Software, Validation.
K. Govardhan: Original draft, editing, Writing- review.
M. Kavitha: Editing, Visualization.
A. R. Deepika: Supervision, Visualization.

DATA AVAILABILITY STATEMENT

The authors confirm that the data that supports the findings of this study are available within the article. Raw data that support the finding of this study are available from the corresponding author, upon reasonable request.

CONFLICT OF INTEREST

The author declared no potential conflicts of interest with respect to the research, authorship, and/or publication of this article.

ETHICS

There are no ethical issues with the publication of this manuscript.

STATEMENT ON THE USE OF ARTIFICIAL INTELLIGENCE

Artificial intelligence was not used in the preparation of the article.

REFERENCES

[1] Sarma AK, Sarma DM, Mudoi S. MHD flow and effects of Hall current, joule heating, and heat source across a chemically reacting and radiating exponentially stretching sheet in a porous medium. Sigma J Eng Nat Sci 2025;43:1179–1196. [CrossRef]

[2] Choi SU, Eastman JA. Enhancing thermal conductivity of fluids with nanoparticles. Argonne National Lab IL (United States) 1997;1997:1–15.

[3] Kaur J, Urvashi G, Sharma RP. Unsteady finite amplitude Magneto-convection of Oldroyd-B Nanofluids with internal heat source. J Nanofluids 2023;12:78–90. [CrossRef]
[4] Sheikholeslami M, Ganji DD. Heat transfer of Cu-water nanofluid flow between parallel plates. Powder Technol 2013;235:873–879. [CrossRef] [
[5] Makinde OD, Eegunjobi AS. MHD flow of a reacting and radiating nanoliquid past an inclined heated permeable plate: Analysis of entropy generation. Latin Am Appl Res 2021;51:269–276. [CrossRef]
[6] Sharma A, Sharma RP. Statistical and numerical analysis of MHD nanofluid (TiO2/EG) flow on a nonlinear curved stretching surface with heat source: A RSM approach. ZAMM 2025;105:1–18. [CrossRef]
[7] Shukla S, Sharma RP, Punith GRJ, Prasannakumara BC. Elastic deformation effect on carboxymethyl cellulose water-based (TiO2-Ti6Al4V) hybrid nano liquid over a stretching sheet with an induced magnetic field. Numer Heat Transf Part A Appl 2023;84:1401–1415. [CrossRef]
[8] Badak K, Sharma RP, Ibrahim SM. A comprehensive study on Maxwell hybrid nanostructure and Maxwell nanostructure on 2D flow model over a stretching sheet with non-uniform heat generation/absorption and binary chemical reaction. J Therm Anal Calorim 2025;150:521–535. [CrossRef]
[9] Sabyasachi M, Ghosh R, Sharma RP. Entropy generation effects on hydromagnetic Williamson nanofluid flow through a porous media. Nanoscience and Nanotechnology Asia 2023;13:1–12. [CrossRef]
[10] Seyyedi SM, Dogonchi AS, Hashemi-Tilehnoee M, Waqas M, Ganji DD. Entropy generation and economic analyses in a nanofluid filled L-shaped enclosure subjected to an oriented magnetic field. Appl Thermal Eng 2020;168:114789. [CrossRef]
[11] Waqas M. Simulation of revised nanofluid model in the stagnation region of cross fluid by expanding-contracting cylinder. International Journal of Numerical Methods for Heat and Fluid Flow 2019;30:2205–2220. [CrossRef]
[12] Dogonchi AS, Hashemi-Tilehnoee M, Waqas M, Seyyedi SM, Animasaun IL, Ganji DD. The influence of different shapes of nanoparticle on Cu-H2O nanofluids in a partially heated irregular wavy enclosure. Physica A Statistical Mechanics and Its Applications 2020;540:123034. [CrossRef]
[13] Sharma RP, Mishra SR. Effect of higher order chemical reaction on magnetohydrodynamic micropolar fluid flow with internal heat source. Int J Fluid Mech Res 2020;47:121–134. [CrossRef]
[14] Tirupathi G, Govardhan K, Nagaraju G, Misra S. MHD upper-convected Maxwell hybrid nanofluid flow over a stretching sheet: A numerical approach. Sigma J Eng Nat Sci 2025;43:1–12. [CrossRef]
[15] Sharma A, Sharma RP. Utilizing neural networks to illustrate the dynamics of viscous fluid flow over curved surface with homogeneous and heterogeneous reactions. Eng Appl Artif Intell 2025;159:111629. [CrossRef]
[16] Sharma RP, Praharaj S, Barik BK, Kumar VV, Sharma A, Mahanta C. Neural network-based analysis of thermal and mass transfer in nanofluid flow through a microchannel under pollutant concentration effect. Multiscale Multidiscip Model Exp Design 2025;8:313–325. [CrossRef]
[17] Wang Q, Qian K, Liu SS, Yang YJ, Liang B, Zheng CS, et al. X-ray visible and uniform alginate microspheres loaded with in situ synthesized BaSO4 nanoparticles for in vivo transcatheter arterial mobilization. Biomacromolecules 2015;16:1240–1246. [CrossRef]
[18] Becker TA, Kipke DR, Brandon T. Calcium alginate gel: A biocompatible and mechanically stable polymer for endovascular embolization. J Biomed Mater Res 2001;54:76–86. [CrossRef]
[19] Tønnesen HH, Karlsen J. Alginate in drug delivery systems. Drug Dev Ind Pharm 2002;28:621-630. [CrossRef]
[20] Giri TK, Thakur D, Alexander A, Badwaik H, Tripathi DK. Alginate based hydrogel as a potential biopolymeric carrier for drug delivery and cell delivery systems: Present status and applications. Curr Drug Deliv 2012;9:539–555. [CrossRef]
[21] Hori Y, Winans AM, Irvine DJ. Modular injectable matrices based on alginate solution/microsphere mixtures that gel in situ and co-deliver immunomodulatory factors. Acta Biomater 2009;5:969–982. [CrossRef]
[22] Akbari S, Pirbodaghi T. Microfluidic encapsulation of cells in alginate particles via an improved internal gelation approach. Microfluid Nanofluidics 2013;16:773–777. [CrossRef]
[23] Zimmermann H, Shirley SG, Zimmermann U. Alginate-based encapsulation of cells: Past, present, and future. Curr Diabetes Rep 2007;7:314–320. [CrossRef]
[24] Martine CJ, Kim JW, Ye C, Ortiz I, Rowat AC, Marquez W, et al. Microfluidic approach to encapsulate living cells in uniform alginate hydrogel microparticles. Macromol Biosci 2012;12:946–951. [CrossRef]
[25] Zhao LB, Pan L, Zhang K, Guo SS, Liu W, Wang Y, et al. Generation of Janus alginate hydrogel particles with magnetic anisotropy for cell encapsulation. Lab Chip 2009;9:2981–2986. [CrossRef]
[26] Barnett BP, Arepally A, Stuber M, Arifin DR, Kraitchman DL, Bulte JMW. Synthesis of magnetic resonance-, X-ray- and ultrasound-visible alginate microcapsules for immune isolation and non-invasive imaging of cellular therapeutics. Nat Protoc 2011;6:1142–1151. [CrossRef]

[27] Sharma RP, Barik BK, Vinay K, Sharma A. Illustration of low oscillating magnetic field on sodium alginate-based hybrid nanofluid flow between two revolving disks: An artificial neural network-based study. Engineering Applications of Artificial Intelligence 2025;155:111101. [CrossRef]

[28] Kumar VV, Sharma RP. Entropy generation minimization in nuclear reactor cooling via rough rotating disk: A statistical approach. Multiscale Multidisciplinary Model Exp Design 2025;245:8–15. [CrossRef]

[29] Reza M, Rana A. Thermofluidic transport of electrohydrodynamic flow of sodium alginate based Casson nanofluid passing through a porous medium under the effect of streaming potential. Int J Eng Technol 2021;10:38–45. [CrossRef]

[30] Alshahrani S, Ahammad NA, Bilal M, Ghoneim ME, Ali A, Yassen MF, et al. Numerical simulation of ternary nanofluid flow with multiple slip and thermal jump conditions. Front Energy Res 2022;10:967307. [CrossRef]

[31] Arif M, Kumam P, Kumam W, Mostafa Z. Heat transfer analysis of radiator using different shaped nanoparticles water-based ternary hybrid nanofluid with applications: A fractional model. Case Stud Therm Eng 2022;31:101837. [CrossRef]

[32] Alharbi KAM, Ahmed AES, Ould Sidi M, Ahammad NA, Mohamed A, Abdullah M, et al. Computational valuation of Darcy ternary-hybrid nanofluid flow across an extending cylinder with induction effects. Micromachines 2022;13:588. [CrossRef]

[33] Bilal M, Gul T, Mouldi A, Mukhtar S, Alghamdi W, Bouzgarrou SM, et al. Melting heat transition in a spinning flow of silver-magnesium oxide/engine oil hybrid nanofluid using parametric estimation. J Nanomater 2022;2022:1–13. [CrossRef]

[34] Guedri K, Khan A, Sene N, Raizah Z, Saeed A, Galal A. Thermal flow for radiative ternary hybrid nanofluid over nonlinear stretching sheet subject to Darcy-Forchheimer phenomenon. Math Problems Eng 2022;2022:3429439. [CrossRef]

[35] Jagadish VT, Guled CN, Noeiaghdam S, Fernandez-Gamiz U, Govindan V, Balamuralitharan S. Effects of thermophoresis and Brownian motion for thermal and chemically reacting Casson nanofluid flow over a linearly stretching sheet. Results in Engineering 2022;15:100448. [CrossRef]

[36] Deepika AR, Govardhan K, Rana A, Reza M. Soret and Dufour effects on MHD mixed convection flow of Casson hybrid nanofluid over a permeable stretching sheet. International Journal of Ambient Energy 2023;44:2115–2127. [CrossRef]

[37] Reza M, Bhattacharyya A, Rana A, Patra R. Soret and Dufour effects on entropy generation for AlN and hybrid nanofluid flow over past a stretching sheet in porous media. In: Proceedings of the 65th Congress of ISTAM. IIT Bhubaneswar: ISTAM; 2020. p. 1–10.

[38] Reddy PS, Chamkha AJ. Soret and Dufour effects on MHD convective flow of Al2O3-water and TiO2-water nanofluids past a stretching sheet in porous media with heat generation/absorption. Advanced Powder Technology 2016;27:1207–1218. [CrossRef]

[39] Okasha MM, Abbas M, Fateh HM, Ameen S, Salah F, Abbas A, et al. Applications of Casson tetra hybrid nanofluid in industrial cooling systems: An investigation of radiative flow and Stephan blowing impacts. J Radiat Res Appl Sci 2025;18:101300. [CrossRef]

[40] Sohail M, Essam REZ, Mousa AAA, Nazir U, Althobaiti S, Althobaiti A, et al. Finite element analysis for ternary hybrid nanoparticles on thermal enhancement in pseudo-plastic liquid through porous stretching sheet. Sci Rep 2022;12:9219. [CrossRef]

[41] Wang G, Zhang Z, Wang R, Zhu Z. A review on heat transfer of nanofluids by applied electric field or magnetic field. Nanomaterials 2020;10:2386. [CrossRef]

[42] Sajjan K, Ahammad NA, Raju CSK, Prasad MK, Shah NA, Botmart T. Study of non-linear thermal convection of ternary nanofluid within Darcy-Brinkman porous structure with time dependent heat source/sink. Mathematics 2022;8:4237–4260. [CrossRef]